DYNAMIC RESPONSE ANALYSIS OF OFFSHORE FLOATING HOSE STRINGS UNDER WAVE LOAD

Reference NO. IJME 645, DOI: 10.5750/ijme.v164iA4.1249

C An, D W Zhao, Y Gao, and **Y Yang,** College of Safety and Ocean Engineering, China University of Petroleum-Beijing, Beijing 102249, China; **T T LI*,** National Science Library, Chinese Academy of Sciences, Beijing 100190, China

KEY DATES: Submitted: 15/05/20; Final acceptance: 11/10/22; Published: 27/03/23

* Correspondence: litongtong@mail.las.ac.cn

SUMMARY

A floating hose is key item for offshore oil transportation. In this paper, a mathematical model is derived for the overall dynamic performance of a single point-moored floating hose string under wave and current load. Airy wave theory was selected to calculate the wave force on the floating hose string. The dynamics of buoy, floating hose string and FSO were modelled using elastic foundation beam theory and discretised by using a fixed grid finite difference method. Discontinuities in the bending stiffness due to the flange connections are also considered. To verify the accuracy of the mathematical model, the finite element model of the buoy, floating hose string and FSO as a system was established by use of Orcaflex software tool. Numerical results for the displacement and bending moment at each section of the floating hose under severe sea conditions were obtained.

KEYWORDS

Floating hose; Dynamic response; Mathematical model; Orcaflex

NOMENCLATURE

B	*buoyancy per unit length of the floating hose*
B_{max}	*maximum buoyancy force per unit length*
E	*elastic modulus of the floating hose*
g	*Acceleration due to gravity (9.81m/s^2)*
H_h	*amplitude of heave of the buoy*
H_p	*amplitude of pitching of the buoy*
I	*moment of inertia of the floating hose section*
k	*wave numbers*
K	*slope of the approximate linear section*
L	*overall length of the floating hose string*
M	*moment value at the section of the floating hose*
N	*nodes number*
q	*wave load*
r	*outer diameter of the hose section*
W	*gravity per unit length of the floating hose*
Y_e	*initial elevation of the FSO-hose interface above sea level*
Y_p	*equilibrium position of the hose central axis from sea level*
ε	*phase angle*
ε_h	*phase angle between the wave and the buoy*
θ_e	*inclination angle between the FSO-hose interface and the horizontal plane*
k	*differential quantity of time*
ρ_w	*seawater density*
ω	*wave frequency*

1. INTRODUCTION

A floating hose is an important item for crude oil transportation between the hull and buoys in an FSO system due to its advantages of light weight, high tensile strength, and ability to achieve rapid deployment and withdrawal (Tonatto *et al.* 2016; O'Donoghue and Halliwell, 1990). In order to meet the strength, flexibility and buoyancy requirement, a floating hose is composed by an elastomeric layer for lining, reinforcing textile fabric and steel wire cord layers impregnated with elastomers for the main body, a closed cell foam material for the buoyancy layer, and an elastomeric layer the for cover.

Most of the published studies on floating hose focused on the static mechanical behavior of floating hose under various loading conditions, such as tension, bending, internal pressure, torsion. Tonatto *et al.* (2016) developed a finite element progressive damage model based on Multi-Continuum Theory to predict crushing strength of the central section of the floating hose. Tonatto *et al*. (2018) presented a nonlinear finite element model to evaluate the axial, bending and torsional stiffnesses of floating double carcass marine hose with hybrid polyaramid/polyamide reinforcement cords. Based on the anisotropic laminated composite theory, Zhou *et al.* (2018) performed an analytical study on reinforcement layers of bonded flexible marine hose under internal pressure. Gao *et al.* (2018) created a nonlinear finite element model to predict the structural behavior of the single carcass composite hose under internal pressure. Besides, Tonatto *et al.* (2017)

established the finite element models to predict the burst pressure of the double carcass floating hose.

The floating hoses are constantly subjected to the dynamic forces of the sea which can result in severe loads and stresses exerting on the hoses. A thorough examination of dynamic behaviors of the floating hose strings subjected to wave action should be undertaken to understand the stress distribution and the hose movement. By establishing the partially immersed cylinder model which simulated the morphologic and mechanical characteristics of floating hose, Zhang *et al.* (2015) presented an improved Morison equation for the wave load of offshore floating hose. Based on hydraulic model tests and analytical study, O'Donoghue and Halliwell (1990) examined the axial forces and vertical bending moments of the floating hose string induced by the combined action of waves and buoy motions. Brown and Elliott (1988) presented a mathematical model and the corresponding numerical method for the dynamic analysis of marine hoses subjected to both wave and buoy action. By using in-house program ANFLEX, Roveri *et al.* (2002) created a coupled model of the buoy, mooring system, submarine and floating hose to analyse the force response of the CALM system floating hose. Tonatto et al. (2018) adopted the element formulations and time integration schemes documented in commercial software package Orcaflex to calculate overall forces and moments on the floating hoses. By incorporating the RAOs of the buoy obtained by ANSYS AQWA and key environmental, geometric and material properties, Amaechi *et al.* (2019) developed a dynamic model on the CALM buoy with submarine hose in Chinese-lantern configuration using Orcaflex, and studied the effects of hose hydrodynamic loads and flow angles on the structural behavior of the hose.

This paper mainly aims at establishing a mathematical model of a single point-moored floating hose string under wave load obtained through Airy wave theory, considering the in-situ working conditions of the floating hose string. Based on elastic foundation beam theory, the dynamical model of buoy, floating hose string and FSO are discretized by using fixed grid finite difference method. The discontinuity of the bending rigidity caused by the flange connections is also considered. Besides, the finite element model was established by Orcaflex software and compared with the mathematical model to verify its accuracy. The numerical results of displacement and bending moment at each section of floating hose are obtained under various sea conditions.

2. THEORETICAL MODEL

In this chapter, a dynamic mathematical model (Dyke *et al.*, 1985) of the floating hose string assembly coupling buoy and FSO is derived, considering the deformation and stress of the floating hose string assembly under wave load with the boundary conditions provided by the CALM buoy and FSO coupling.

2.1 DIFFERENTIAL EQUATION OF BENDING VIBRATION OF FLOATING HOSE STRING UNDER WAVE LOAD

Combined with the dynamic response characteristics of floating hose string in actual sea conditions, the floating hose string can be simplified into a Bernoulli-Euler elastic beam. The motion of the floating hose string under wave current load is assumed to be the bending vibration of an ideal elastic body. Because the horizontal span of the hose is much larger than the height of the hose section, the influence of the shear force in the hose on the bending deformation of the hose is ignored. Therefore, the differential equation of bending deformation of floating hose string under wave load is:

$$\frac{\partial^2 y(x,t)}{\partial^2 x} = \frac{M}{EI} \tag{1}$$

where E is that elastic modulus of the floating hose, I is the moment of inertia of the floating hose section, M represents the moment value at the section of the floating hose at x, $y = y(x, t)$ is the function form of floating hose string deformation curve with respect to time and displacement.

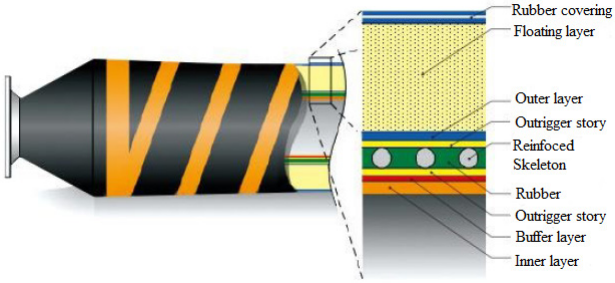

Figure 1. Layer structure of floating hose

As can be seen from that stress diagram of the hose string in Figure 2:

$$\frac{\partial M(x,t)}{\partial x} = Q \tag{2}$$

Substituting Equation (1) into Equation (2), the differential equation of the deformation curve of the floating hose string under the wave load q is obtained:

$$EI\frac{\partial^3 y(x,t)}{\partial x^3} = Q \tag{3}$$

Motion equation of micro-segment hose string dx along y-axis direction:

$$Q - \left(Q + \frac{\partial Q}{\partial x}dx\right) + qdx = mdx\frac{\partial^2 y(x,t)}{\partial t^2} \tag{4}$$

where the mass per unit length on the floating hose is m, acceleration is $\frac{\partial^2 y(x,t)}{\partial t^2}$.

Substituting Equation (3) into Equation (4), the differential equation of bending vibration of the hose string under wave load is obtained:

$$\frac{\partial^4 y(x,t)}{\partial x^4}+\frac{1}{\alpha^2}\frac{\partial^2 y(x,t)}{\partial t^2}=F \tag{5}$$

Where,

$$\alpha^2=\frac{EI}{m};\ F=\frac{q}{EI} \tag{6}$$

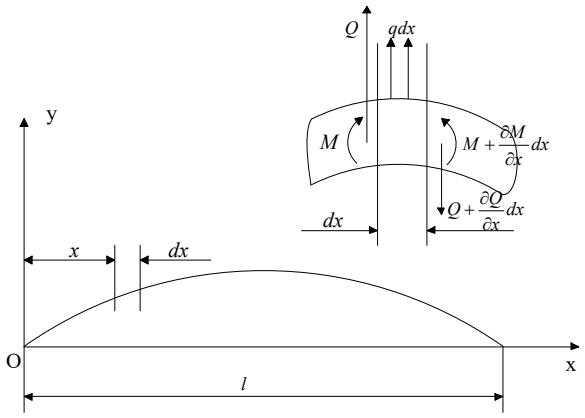

Figure 2. The force analysis of floating hose string

2.2 ENVIRONMENTAL LOAD

In order to calculate the effect of wave load on the floating hose, the appropriate wave theory should be selected for calculation first. According to DNV report (2007), this paper selects the commonly used parameters of the East China Sea and selects the wave theory as the linear wave theory as suggested by DNV (2007).

Linear wave waveform formula is:

$$\eta(x,t)=\frac{H}{2}\cos(kx-\omega t) \tag{7}$$

where H is the wave height; k is the wave number; ω is the wave frequency; t is the time after the peak passes through the origin.

Considering that wave load acts on the floating hose, the floating hose string is affected by its own gravity, sea water buoyancy and wave load in the vertical plane. The dynamic load of floating hose string is approximately calculated by elastic foundation theory. Dunlop and Bridgestone used the elastic foundation theory to calculate the static load of the floating hose string approximately. Under the static load, the floating hose string only receives its own gravity and seawater buoyancy in the vertical plane. Take the z axis as sea level, the O point is located on the axis of the hose string, x is the axis of the hose string, and y is the vertical distance from the axis of the hose string to sea level, as shown in Figure 3.

The volume per unit length of the hose string immersed in seawater is:

$$V=r^2(\pi-\alpha)+S_{AOB}=r^2(\pi-\alpha)+y^2\tan\alpha \tag{8}$$

Static load per unit length hose string is:

$$Q=W-B=W-\rho_w gV \tag{9}$$

where Q is the static load per unit length of the floating hose string without wave flow, W is the gravity per unit length of the floating hose, B is the buoyancy per unit length of the floating hose. ρ_w is the seawater density, g is the gravity acceleration, r is the outer diameter of the hose section.

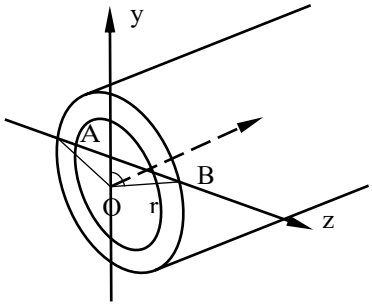

Figure 3. Schematic diagram of the hose string floating

According to Equation (9) and common structural parameters of the hose, the load curve of the hose string can be drawn. Without affecting the calculation accuracy, the floating load of the hose is equivalent to a linear relationship in the range of $-r\le y\le r$. Equation (9) can be simplified as:

$$Q=W-K(y+r)\ \ when -r\le y\le r,$$

$$K=\frac{B_{max}}{2r};\ B_{max}=\rho_w g\pi r^2 \tag{10}$$

where K is the slope of the approximate linear section, and B_{max} is the maximum buoyancy force per unit length of the floating hose (all immersed in seawater).

Under static load, when the buoyancy force on the hose is equal to gravity, the equilibrium position y_p of the hose central axis from sea level is obtained, making $Q=0$:

$$y_p=\frac{W}{K}-r=\frac{2W}{\rho_w g\pi r}-r \tag{11}$$

The stress of the hose under static load is equivalent to the direct proportional relationship between the axial position of the hose and the difference between the equilibrium positions:

$$Q = -Ky^*, y^* = y - y_p \tag{12}$$

Similarly, considering the wave load acting on the floating hose, the dynamic load of the floating hose is approximately calculated by using the elastic foundation theory:

$$Q = W - K\left(r + y - \eta\right) \; when - r \le y - \eta \le r \tag{13}$$

where $y - \eta$ is the distance between the axial position of the hose and the wave surface.

Also,

$$q = -K\left[y\left(x,t\right) - \eta\left(x,t\right) - y_p\right] \tag{14}$$

$$q = -K\left[y\left(x,t\right) - \frac{H}{2}\cos\left(kx - \omega t\right) - y_p\right] \tag{15}$$

2.3 BUOY BOUNDARY CONDITION

When only considering that the buoy interface and the floating hose string port are in the same vertical plane, only the heaving and pitching of the buoy under the action of waves will affect the boundary conditions of the buoy–hose interface. The heave of buoy affects the initial displacement of the interface and the phase angle (ε) between buoy and wave. Let the initial displacement of the buoy–hose interface from the horizontal plane be y_0. Under the action of wave load, the phase angle between the wave and the buoy is ε_h when the buoy generates heave motion. Take the phase angle $\varepsilon_h = 0$. When the buoy generates heave motion, the amplitude of heave of the buoy is H_h. Let $kx' = \varepsilon_h$:

$$x' = \frac{\varepsilon_h}{k} \tag{16}$$

The Equation (21) is brought into the linear wave surface Equation (12) to obtain:

$$\begin{cases} y\left(x = 0\right) = y_0 + \eta\left(x' = \dfrac{\varepsilon_h}{k}\right) \\ y\left(x = 0, t\right) = y_0 + \dfrac{H_h}{2}\cos\left(-\omega t\right) \end{cases} \tag{17}$$

The pitch of buoy affects the inclination angle of the interface $\theta\left(x,t\right)$. Under the action of wave load, the phase angle between wave and buoy is ε_p. When the buoy generates pitching motion, the amplitude of pitching of the buoy is H_p. Let $kx' = \varepsilon_p$:

$$x' = \frac{\varepsilon_p}{k} \tag{18}$$

The Equation (18) is brought into the linear wave surface Equation (7) to obtain:

$$\begin{cases} \theta\left(x = 0\right) = \theta_0 + \dfrac{\partial\eta}{\partial x}\left(x' = \dfrac{\varepsilon_p}{k}\right) \\ \theta\left(x = 0\right) = \theta_0 + \dfrac{H_p}{2}k\sin\left(-\omega t\right) \end{cases} \tag{19}$$

where $\theta\left(x,t\right)$ is the angle between the wave surface function $\eta\left(x,t\right)$ and the x axis.

2.4 FSO BOUNDARY CONDITIONS

For the motion of FSO under wave load, this paper only considers the influence of heaves and pitches on FSO. Under the action of wave load, the phase angle between wave and buoy is $\varepsilon_{h'}$. Similarly, let $kx' = \varepsilon_h^{'}$:

$$x' = \frac{\varepsilon_h^{'}}{k} \tag{20}$$

When the FSO produces heave motions, it will affect the elevation of the FSO-hose interface above sea level. The Equation (20) is brought into the linear wave surface Equation (7) to obtain:

$$\begin{cases} y\left(x = L\right) = y_e + \eta\left(x' = \dfrac{\varepsilon_h^{'}}{k}\right) \\ y\left(x = L\right) = y_e + \dfrac{H_h^{'}}{2}\cos\left(-\omega t\right) \end{cases} \tag{21}$$

where y_e is the initial elevation of the FSO-hose interface above sea level, H_h' is the amplitude of buoy heave. θ_e is the inclination angle between the FSO-hose interface and the horizontal plane ($\theta_e = 0$). The phase angle between the wave and the FSO is $\varepsilon_p^{'}$. The pitch motion of FSO affects the inclination angle of the FSO-hose interface $\theta\left(x,t\right)$. Let $kx' = \varepsilon_p^{'}$:

$$x' = \frac{\varepsilon_p^{'}}{k} \tag{22}$$

The Equation (22) is brought into the linear wave surface Equation (7) to obtain:

$$\begin{cases} \theta\left(x = L\right) = \theta_e + \dfrac{\partial\eta}{\partial x}\left(x' = \dfrac{\varepsilon_p^{'}}{k}\right) \\ \theta\left(x = L\right) = \theta_e + \dfrac{H_p^{'}}{2}k\sin\left(-\omega t\right) \end{cases} \tag{23}$$

where $H_p^{'}$ is the amplitude of buoy pitching.

3. NUMERICAL SOLUTION

3.1 SINGLE FLOATING HOSE

In this paper, the fixed-grid finite-difference method proposed by O'Donoghe and Halliwell in 1990 is used in

the vertical solution process. The numerical value of the bending vibration curve equation $y(x,t)$ of the floating hose at any position on the hose and at any time (x_i, t_j) can be expressed as follows:

$$\begin{cases} y(x_i,t_j) = y(ih,jk) = y_{i,j} \\ x_i = 0 + ih = ih;\ i = 1,2,3\ldots N \\ t_j = 0 + j\kappa = j\kappa;\ j \geq 0 \end{cases} \quad (24)$$

$$h = \delta x = \frac{L}{N+1},\ x \in (0,L);\ \kappa = \delta t, t \in [0,+\infty) \quad (25)$$

where L is the overall length of the floating hose string, x_i and t_j are nodes, N is the number of equidistant nodes in the interval [0, L].

Discretization of differential equations into difference equations. The central difference scheme will lead to instability in the solution of the above-mentioned hose differential equations (Brown and Elliott, 1988), so the backward difference scheme is adopted in this paper.

$$\left(\frac{\partial^4 y(x,t)}{\partial x^4}\right)_{i,j+1} + \left(\frac{1}{\alpha^2}\frac{\partial^2 y(x,t)}{\partial t^2}\right)_{i,j+1} = F_{i,j+1} \quad (26)$$

$$\left(\frac{\partial^2 y(x,t)}{\partial t^2}\right)_{i,j+1} = \frac{y_{i,j+1} - 2y_{i,j} + y_{i,j-1}}{k^2} + O(k^2) \quad (27)$$

$$\left(\frac{\partial^4 y(x,t)}{\partial x^4}\right)_{i,j+1} = \frac{y_{i+2,j+1} - 4y_{i+1,j+1} + 6y_{i,j+1} - 4y_{i-1,j+1} + y_{i-2,j+1}}{h^4} + O(h^2) \quad (28)$$

Substituting Equations (27) and (28) into Equation (26):

$$\frac{y_{i+2,j+1} - 4y_{i+1,j+1} + 6y_{i,j+1} - 4y_{i-1,j+1} + y_{i-2,j+1}}{h^4} + \frac{1}{\alpha^2}\frac{y_{i,j+1} - 2y_{i,j} + y_{i,j-1}}{k^2} = F_{i,j+1} \quad (29)$$

$$F_{i,j+1} = \frac{q_{i,j+1}}{EI} = -\frac{K}{EI}\left[y_{i.j+1} - \frac{H}{2}\cos(kih - \omega(j+1)\kappa) - y_p\right] \quad (30)$$

$$ey_{i+2,j+1} - 4ey_{i+1,j+1} + \gamma y_{i,j+1} - 4ey_{i-1,j+1} + ey_{i-2,j+1} = \frac{1}{\alpha^2\kappa^2}(2y_{i,j} - y_{i,j-1}) + \frac{K}{EI}\left[\frac{H}{2}\cos(kih - \omega(j+1)\kappa) + y_p\right] \quad (31a)$$

Where,

$$e = \frac{1}{h^4};\ \gamma = \frac{6}{h^4} + \frac{1}{\alpha^2\kappa^2} + \frac{K}{EI};\ b_{i,j+1} = \frac{1}{\alpha^2\kappa^2}(2y_{i,j} - y_{i,j-1}) \quad (31b)$$

Let $b_{i,j+1} = \frac{1}{\alpha^2\kappa^2}(2y_{i,j} - y_{i,j-1})$, and according to Equation (17):

$$b_{i,j+1} = \frac{1}{\alpha^2\kappa^2}\left[y_0 + H\cos(-\omega j\kappa) - \frac{H}{2}\cos(-\omega(j-1)\kappa)\right] \quad (32)$$

Let

$$f_{i,j+1} = \frac{1}{\alpha^2\kappa^2}(2y_{i,j} - y_{i,j-1}) + \frac{K}{EI}\left[\frac{H}{2}\cos(kih - \omega(j+1)\kappa) + y_p\right],$$

and Equation (36) is equivalent to:

$$ey_{i+2,j+1} - 4ey_{i+1,j+1} + \gamma y_{i,j+1} - 4ey_{i-1,j+1} + ey_{i-2,j+1} = f_{i,j+1} \quad (33)$$

Combine the boundary conditions at the pontoon, according to Equation (18) and Equation (20):

$$y_{0,j+1} = y_0 + \frac{H_h}{2}\cos(-\omega t), \quad when\ x = 0, i = 0 \quad (34)$$

Using the first-order center difference quotient formula

$$\frac{y_{1,j+1} - y_{-1,j+1}}{2h} = y'_{0,j+1},$$

$$y_{1,j+1} - y_{-1,j+1} = 2h\frac{\partial \eta}{\partial x}\left(x' = \frac{\varepsilon_h}{k}\right) = hH_h k\sin(-\omega t) \quad (35)$$

Combine the boundary conditions at the FSO, according to Equation (21):

$$y_{N+1,j+1} = y_e + \frac{H'_h}{2}\cos(-\omega t) \quad (36)$$

Using the first-order center difference quotient formula

$$\frac{y_{N+2,j+1} - y_{N,j+1}}{2h} = y'_{N+1,j+1},$$

$$y_{N+2,j+1} - y_{N,j+1} = 2h\frac{H'_h}{2}k\sin(-\omega t) = hH'_h k\sin(-\omega t) \quad (37)$$

The difference equations are obtained from Equations (33), (34), (35), (36) and (37). Write the system of difference equations into a matrix:

$$Ay^T_{j+1} = f^T_{j+1} \quad (38)$$

Where,

$$A = \begin{vmatrix} -1 & 0 & 1 & 0 & 0 & & & & & & & & \\ 0 & 1 & 0 & 0 & 0 & & & & & & & & \\ e & -4e & \gamma & -4e & e & 0 & & & & & & & \\ 0 & e & -4e & \gamma & -4e & e & 0 & & & & & & \\ \cdots & \cdots & \cdots & \cdots & \cdots & \cdots & \cdots & \cdots & \cdots & \cdots & \cdots & \cdots & \cdots \\ & & & & & & & 0 & e & -4e & \gamma & -4e & e \\ & & & & & & & & & 0 & 0 & 1 & 0 \\ & & & & & & & & & & -1 & 0 & 1 \end{vmatrix} \quad (39)$$

$$y^T_{j+1} = (y_{-1,j+1}, y_{0,j+1}, \cdots, y_{N+1,j+1}, y_{N+2,j+1}) \quad (40)$$

$$f_{j+1}^{T}=\begin{pmatrix} hH_h k\sin(-\omega t), y_0+\frac{H_h}{2}\cos(-\omega t), \\ f_{1,j+1},\cdots,f_{N,j+1}, y_e+\frac{H_h^{'}}{2}\cos(-\omega t), hH_h^{'}k\sin(-\omega t)\end{pmatrix} \quad (41)$$

3.2 INFLUENCE OF FLANGE FITTINGS

Due to the different materials and structures of the flange and the hose body and the different bending rigidity, the bending rigidity of the floating hose connected by the flange is discontinuous at the joint of the flange and the hose, and the discontinuity of the bending rigidity affects the second derivative and the higher derivative of the deformation function to the displacement. At the joint of flange and hose, the displacement and the deformation slopes of flange and hose are equal. It can be further known from formula $\frac{\partial^2 y(x,t)}{\partial x^2}=\frac{M}{EI}$ that the bending moments they bear are also equal:

$$y_r(x,t)=y_s(x,t) \quad (42)$$

$$\frac{\partial \mathrm{y_r}(x,t)}{\partial \mathrm{x}}=\frac{\partial \mathrm{y_s}(x,t)}{\partial \mathrm{x}} \quad (43)$$

$$M=\frac{\partial^2 y_r(x,t)}{\partial^2 x}EI_r=EI_s\frac{\partial^2 y_s(x,t)}{\partial^2 x} \quad (44)$$

$$\frac{\partial^2 y_r(x,t)}{\partial^2 x}=R\frac{\partial^2 y_s(x,t)}{\partial^2 x}\ where\ R=\frac{EI_s}{EI_r} \quad (45)$$

where r stands for rubber hose, s stands for flange fitting steel structure.

The discontinuity of bending stiffness can be seen from Equation (43). Considering the influence of discontinuity, five points $x_i=x_0+ih,\ h=x-x_0\,(i=-2,-1,0,1,2)$ are introduced in this paper. Take $i=0$ at the flange and hose interface, take $i=-2,-1$ for the hose close to the interface, and take $i=2,1$ at the flange close to the interface. $\mathrm{y}(x_1,t)$ and $\mathrm{y}(x_2,t)$ are expanded by Taylor series at $x=x_0$:

$$y(x_{-1},t)=y(x_0,t)-h\frac{\partial y_r(x_0,t)}{\partial x}+\frac{h^2}{2!}\frac{\partial^2 y_r(x_0,t)}{\partial x^2} \quad (46)$$

$$y(x_1,t)=y(x_0,t)+h\frac{\partial y_s(x_0,t)}{\partial x}+\frac{h^2}{2!}\frac{\partial^2 y_s(x_0,t)}{\partial x^2} \quad (47)$$

According to Equations (42) and (44):

$$y(x_1,t)=y(x_0,t)+h\frac{\partial y_r(x_0,t)}{\partial x}+\frac{1}{R}\frac{h^2}{2!}\frac{\partial^2 y_r(x_0,t)}{\partial x^2} \quad (48)$$

Use the difference formula $\left(\frac{\partial y^2(x,t)}{\partial h^2}\right)_{i,j+1}=\frac{y_{i+1,j+1}-2y_{i,j+1}+y_{i-1,j+1}}{h^2}$ according to the Equations (46):

$$y(x_1,t)=\frac{(2R-2)y(x_0,t)+(1-R)y(x_{-1},t)}{R-1} \quad (49)$$

Similarly, use the difference formula according to the expressions of $y(-2,t)$ and $y(2,t)$:

$$y(x_2,t)=\frac{-2R-4}{R}y(x_0,t)+\frac{2R+2}{R}\left(y(x_1,t)+y(x_{-1},t)\right)-y(x_{-2},t) \quad (50)$$

When time takes $t=j+1$, the number of multiple parallel hoses is taken as N=10, the overall displacement of the hose under wave load obtained by Equations (38) is

$$\left\{\begin{matrix} y_{-1,j+1}, y_{0,j+1}, y_{1,j+1}, y_{2,j+1}, \cdots, \\ y_{N,j+1}, y_{N+1,j+1}, y_{N+2,j+1}\end{matrix}\right\} \quad (51)$$

Then that hose is calculated in section, each hose is provided with left and right flanges, and the influence of the left and right flanges on the hose is calculated respectively. Considering that on the tail hose connecting to the FSO, part of the hose is suspended between the FSO and the sea surface without receiving wave load. In the extracted overall displacement data of the hose, the partial displacement after the hose connected with the FSO is eliminated. This distance is calculated based on the height of the FSO from the sea surface $(H_0=7\ m)$ and the movement of the FSO-hose interface (Sayed and Patel, 1992).

$$y_N=H_0+\frac{H_p^{'}}{2}\cos(\omega t) \quad (52)$$

$$y(x)=-\frac{qx}{24EI}\left(l^3-2lx^2+x^3\right) \quad (53)$$

4. RESULTS AND DISCUSSIONS

In this section, the mathematical model is numerically solved and verified through Orcaflex simulation. The rotary table mooring form of most mooring buoy structures (cylindrical buoys) in practical application is selected, and the general properties of mooring buoys given in Table 1. The general properties of FSO is given in Table 2. The operating parameters of the floating hose are shown in Table 3, and its material parameters are shown in Table 4. Environmental parameters under different working conditions will have a great impact on the oil loading and unloading system. The sea state parameters selected in this paper are 50-year return period. The specific values are shown in Table 5, and the selection of wave parameters and water depth is completed respectively according to Table 5.

Table 1: General properties of CALM.

Parameter	Data	Unit
Diameter	11.0	m
Moulded depth	5.30	m
Draught	2.5	m
Total weight of buoy	250.0	t
Mass moment of inertia x	2411.50	t·m^2
Mass moment of inertia y	2411.50	t·m^2
Mass moment of inertia z	3781.20	t·m^2
Depth of floating hose	0.5	m
Angle with floating hose	15	Deg
Number of catenary anchor legs	6	-
Pre-opening angle	50±2	Deg

Table 2: General properties of FSO.

Parameter	Data	Unit
Length	103.0	m
Width	16	m
Height	13.2	m
Moulded depth	7.30	m
Draught	4.5	m
Total weight	9017.95	t
Mass moment of inertia *x*	254.93e3	t·m^2
Mass moment of inertia *y*	5.980e6	t·m^2
Mass moment of inertia *z*	5.980e6	t·m^2

Table 3: Operating parameters of floating hose.

Operating parameters	Data	Unit
Application standard	OCIMF2008	-
Pressure rating	1.5	MPa
Factory test pressure	1.5	MPa
Minimum burst pressure	7.5	MPa
Allowable operating pressure	−0.075	MPa
Allowable flow rate	13	m/s
Allowable temperature	−20~80	℃
Allowable ambient temperature	−29~52	℃

Table 4: Floating hose parameters.

Parameters	Data	Unit
Length per section	10	m
Inner-diameter	0.365	m
External diameter	0.469	m
Weight per unit length	518.5	kg/m
Bending Stiffness	400	kN/m^2
Axial Stiffness	20000	kN/m
Minimum bending radius	1.956	m

Table 5: Environment parameters.

Environmental parameters	Data	Unit
Depth of water	85	m
50-year high tide	2.5	m
50-year low tide	−2.25	m
Wave height	2	m
Period	5.61	s
Wave direction	0	Deg
Wavelength	20	m

4.1 COMPUTATION OF VERTICAL DISPLACEMENT

Calculation results of vertical displacement of axis of floating hose string are presented in Figure 4. Using MATLAB software to calculate (take wavelength $L = 20\ m$), according to the calculation results in one wave period, the dynamic displacement in the whole vertical plane of the hose string is extracted, and four times t_1, t_2, t_3 and t_4. are respectively selected to fit the displacement curve of the floating hose string. At time $t_1 = 0$ s (Figure 4a), affected by wave load and dynamic boundary, in the vertical displacement of the hose string axis, the displacement of both ends of the hose string is $y = -0.18$ m at $x = 0$ m and $y = 7.5$ m at $x = 100$ m.

Since most of the tail hoses are not subjected to wave loads, the data of the tail hoses are not considered, and the hose string has a maximum displacement $y = 1.1$ m at $x = 4$ m. Similarly, at time $t_2 = 1.4$ s (Figure 4b), in the displacement of the hose string axis in the vertical direction, the displacement of both ends of the hose string is $y = -0.73$ m at $x = 0$ m, $y = 6.1$ m at $x = 100$ m, the maximum displacement occurs at $x = 49$ m, and the displacement $y = -0.75$ m.

At time $t_3 = 2.8$ s (Figure 4c), the axis of the hose string is displaced in the vertical direction, the displacement of both ends of the hose string is $y = -1.1$ m at $x = 0$ m, $y = 6.5$ m at $x = 100$ m, the maximum displacement occurs at

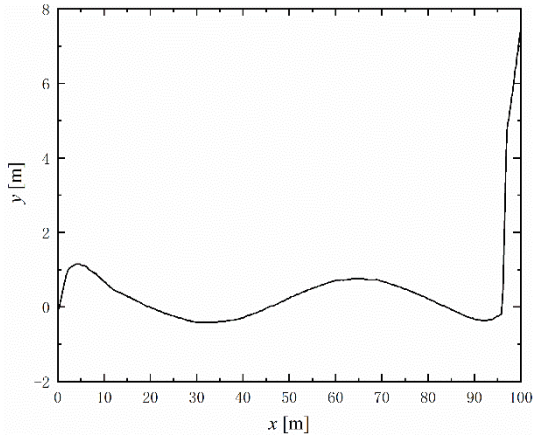

a) at time $t = 0$ s

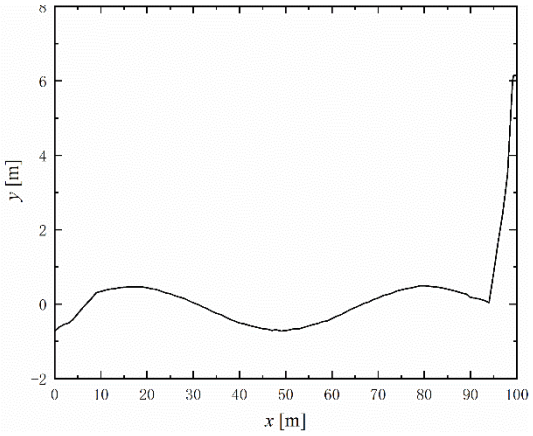

b) at time t = 1.4 s

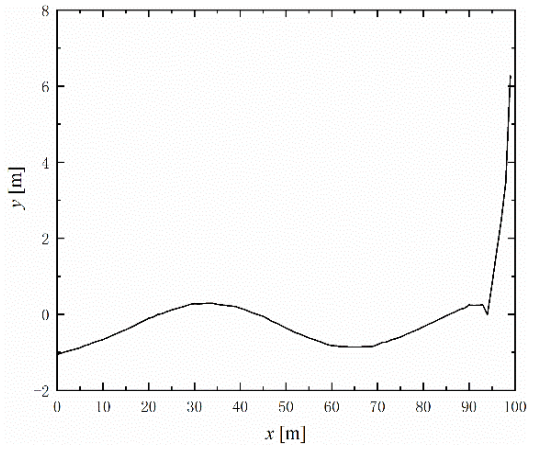

c) at time t = 2.8 s

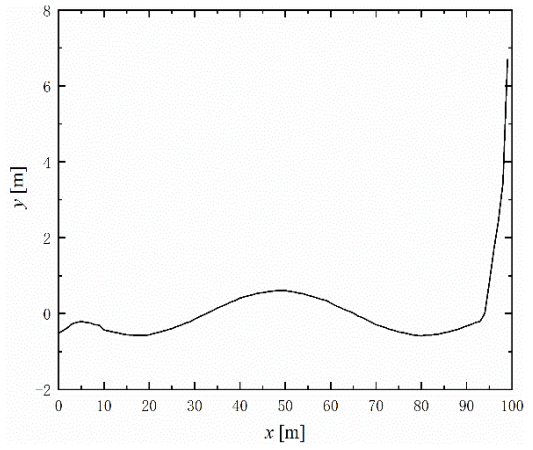

d) at time t = 4.2 s

Figure 4. Vertical displacement diagram of the floating hose string

$x = 0$ m, and $y = -1.1$ m. At time $t_4 = 4.2$ s (Figure 4d), the axis of the hose string is displaced in the vertical direction, the displacement at both ends of the hose string is $y = -0.50$ m at $x = 0$ m, $y = 6.8$ m at $x = 100$ m, the maximum displacement occurs at $x = 80$ m, and the displacement $y = -0.60$ m.

4.2 COMPUTATION OF VERTICAL BENDING MOMENT

From the differential equation of deformation curve $\frac{\partial^2 y(x,t)}{\partial x^2} = \frac{M}{EI}$, one obtaines:

$$M(x,t) = EI\frac{\partial^2 y(x,t)}{\partial x^2} \tag{54}$$

$$M_{i,j+1} = EI\left(\frac{\partial^2 y(x,t)}{\partial x^2}\right)_{i,j+1} = EI\frac{y_{i+1,j+1} - 2y_{i,j+1} + y_{i-1,j+1}}{h^2}$$

$$when\, x = i,\ t = j+1 \tag{55}$$

The connection end of the head hose and the single-point buoy is a reinforced end, and the bending rigidity at the flange is taken as $EI_0 = 2000 kNm^2$:

$$M_{0,j+1} = EI_0\left(\frac{y_{1,j+1} - 2y_{0,j+1} + y_{-1,j+1}}{h^2}\right) when\ \ x = 0 \tag{56}$$

The bending moment curve of the hose string axis is shown in Figure 5. When $t_1 = 0$ s (Figure 5a), displacement coordinate point data $y_{1,0}$, $y_{0,0}$, $y_{-1,0}$ at the left end interface of the head hose of the floating hose string are extracted:

$$M(0,0) = EI_0\left(\frac{y_{1,0} - 2y_{0,0} + y_{-1,0}}{h^2}\right) = 94.3\, kNm \tag{57}$$

At $x = 100$ m, the bending moment $M(100,0) = -35.8$ kNm of the hose string, and the maximum bending moment occurs at $x = 0$ m.

When $t_2 = 1.4$ s (Figure 5b), displacement coordinate point data $y_{1,1.4}$, $y_{0,1.4}$, $y_{-1,1.4}$ at the left end interface of the head hose of the floating hose string are extracted:

$$M(0,1.4) = EI_0\left(\frac{y_{1,1.4} - 2y_{0,1.4} + y_{-1,1.4}}{h^2}\right) = -20.0\, kNm \tag{58}$$

The floating hose string is affected by wave load and dynamic boundary. According to Figure 4b, the bending moment $M(0,1.4) = -20.15$ kNm at $x = 0$ m, $M(100,1.4) = -5.23$ kNm at $x = 100$ m, the maximum bending moment occurs at $x = 92$ m, and the bending moment is $M(94,1.4) = -63.89$ kNm.

Similarly, when $t_3 = 2.8$ s:

$$M(0,2.8) = EI_0\left(\frac{y_{1,2.8} - 2y_{0,2.8} + y_{-1,2.8}}{h^2}\right) = -23.65\, kNm \tag{59}$$

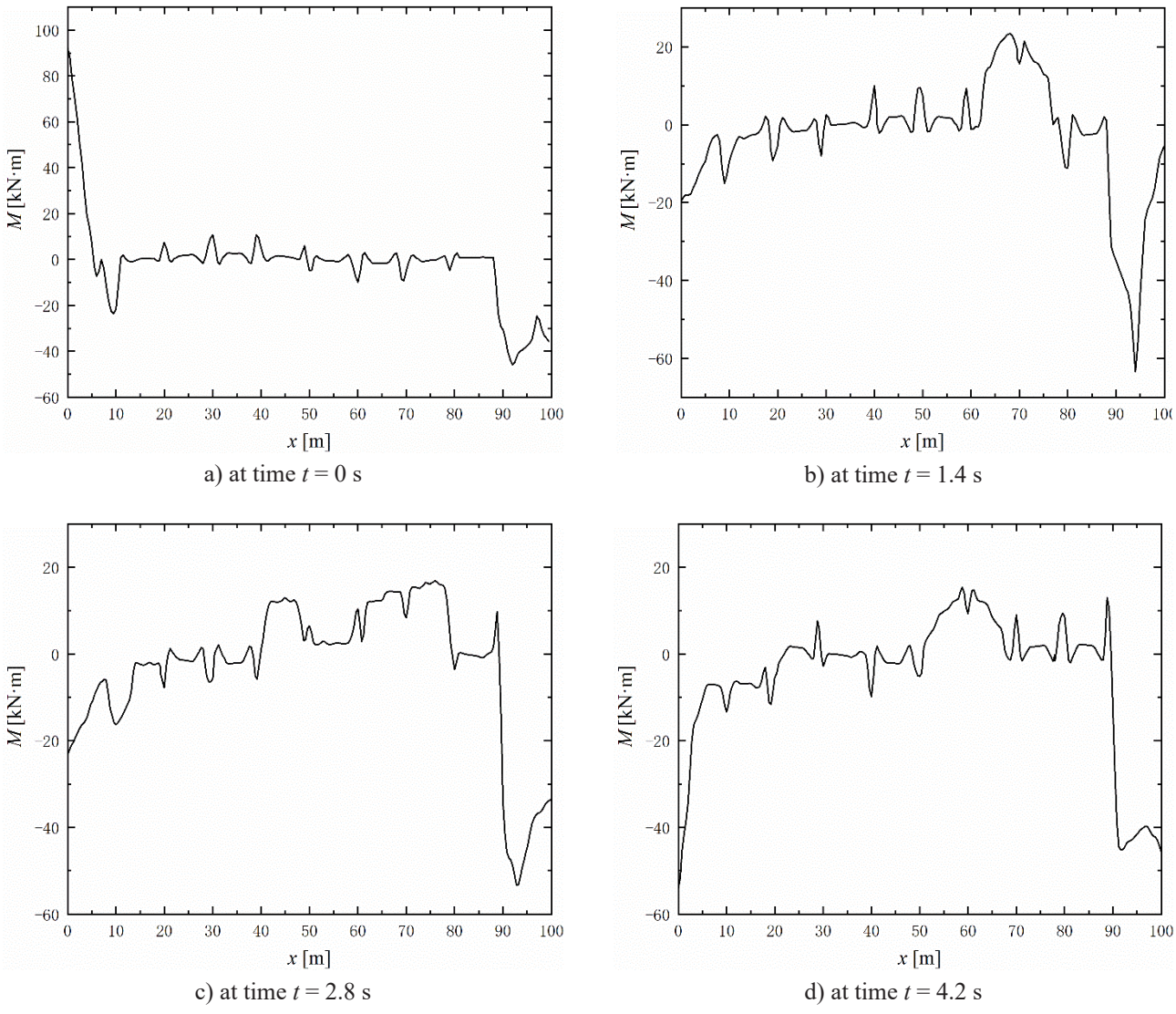

a) at time t = 0 s

b) at time t = 1.4 s

c) at time t = 2.8 s

d) at time t = 4.2 s

Figure 5. Vertical bending moment diagram of the floating hose string

According to Figure 5c, the bending moment $M(0,2.8) = -23.65$ kNm at $x = 0$ m, $M(100,2.8) = -33.2$ kNm at $x = 100$ m, the maximum bending moment occurs at $x = 93$ m, and the bending moment is $M(93,2.8) = -53.8$ kNm. When $t_4 = 4.2$ s:

$$M(0,4.2) = EI_0\left(\frac{y_{1,4.2} - 2y_{0,4.2} + y_{-1,4.2}}{h^2}\right) = -55.68\,kNm \quad (60)$$

According to Figure 4d, the bending moment $M(0,4.2) = -55.68$ kNm at $x = 0$, $M(100,4.2) = -46.38$ kNm at $x = 100$ m, the maximum bending moment occurs at $x = 0$ m, and the bending moment is $M(0,4.2) = -55.68$ kNm.

According to the above results, we can find that there are irregular bending moments at every 10m of the hose, which is due to the large stiffness difference between the flanges at both ends of the hose and the hose tank, resulting in a large change in the axial force of the hose at both ends of the flange and the middle part.

4.3 VERIFICATION THROUGH ORCAFLEX SIMULATION

Firstly, the buoy, FSO and floating hose string are modelled respectively. In Orcaflex software, the buoy, hose string and FSO are connected by flanges in turn to form a complete offshore crude oil loading and unloading system.

Under normal circumstances, the buoy-hose interface is located below the horizontal plane and forms a certain angle with the horizontal plane. In this model, the commonly used angle of is selected, and the buoy and the head hose of the floating hose string are connected through flanges (see Figure 6). The buoy is modelled according to the basic dimensions in Table 6.

Due to the complex structure of the hose, in order to simplify the modeling process and considering the existence of flanges at both ends of the hose, the hose is simplified into three parts: flange, reinforcing layer and inner glue layer for modeling.

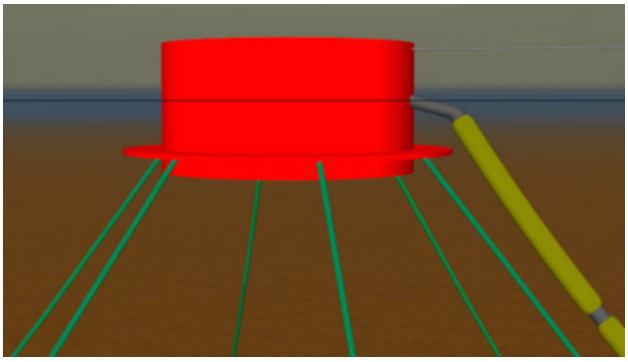

Figure 6. The buoy and floating hose string connection

The main part of the hose is selected as general category line type, which is modelled by common methods, and Profiled line type is selected for the end flange, modeling is conducted by using the homogeneous hose category method (see Figure 7). The hose reinforcement layer has a variable diameter, in this paper, a stiffener attachment is added to the main body of the hose, and the profile of the attachment is the same as that of the end flange (Roveri *et al.*, 2002). Next, ten hoses connected end to end are established to form a floating hose. The left end of the hose is connected to the buoy through a flange, and the right end of the hose is connected with the FSO through a flange.

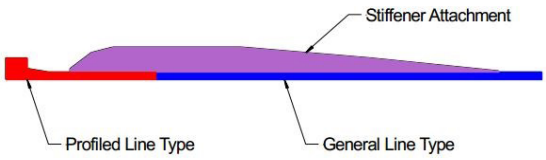

Figure 7. The floating hose modeling equivalent diagram

Connect buoys, hose string and FSO, as shown in Figure 8 to obtain the finite element model of offshore crude oil loading and unloading system.

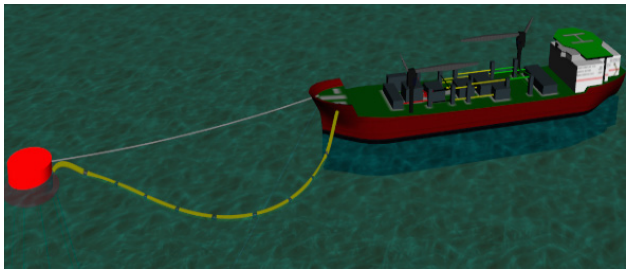

Figure 8. Orcaflex model of offshore crude oil offloading system

According to the established finite element model of offshore crude oil handling system and the settings of the above sea state parameters, the calculation results of Orcaflex software simulation for vertical displacement of hose string axes at four time instants t_1, t_2, t_3 and t_4 are obtained. The comparison between the calculation and simulation results of the vertical displacement of the hose string at four times t_1, t_2, t_3 and t_4 is shown in Figure 9 and Table 6.

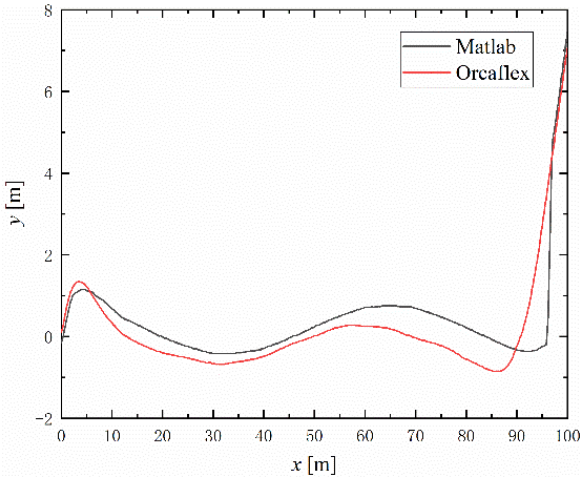

a) at time t = 0 s

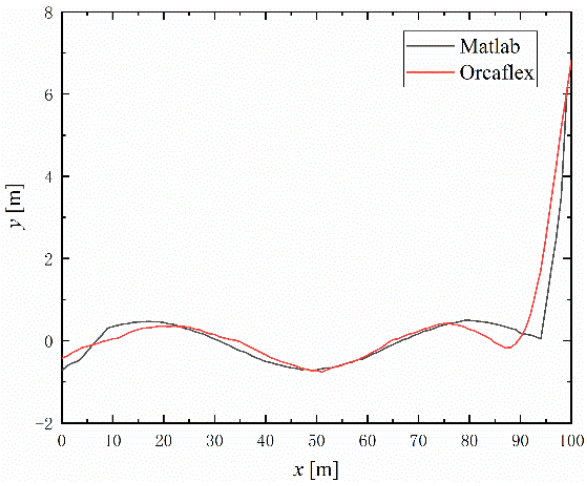

b) at time t = 1.4 s

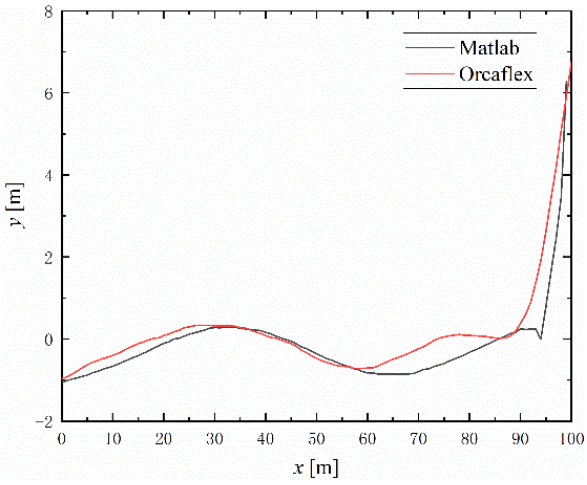

c) at time t = 2.8 s

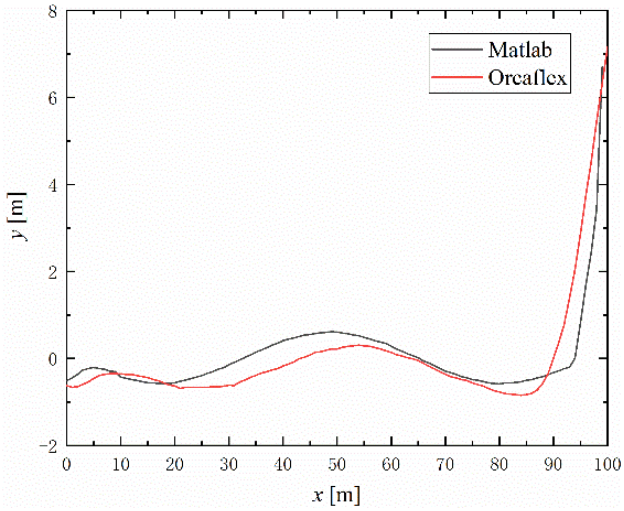

d) at time t = 4.2 s

Figure 9. Vertical displacement comparison diagram of the floating hose string

Table 6: Vertical displacement comparison of the hose string.

	Vertical displacement (m)							
	t_1 = 0 (s)		t_2 = 1.4 (s)		t_3 = 2.8 (s)		t_4 = 4.2 (s)	
	M^a	S^b	M^a	S^b	M^a	S^b	M^a	S^b
x = 0 (m)	−0.18	0.0079	−0.73	−0.46	−1.1	−0.97	−0.50	−0.63
x = 100 (m)	7.5	7.2	6.1	6.8	6.5	6.8	6.8	7.2
Maximum displacement	1.1	1.3	−0.75	−0.75	−1.1	−0.97	−0.60	−0.78

[a] Results obtained by mathematical models. [b] Results obtained by simulation software.

In Orcaflex software, the vertical bending moment values of floating hose string are extracted and simulated into curves. The vertical bending moment of the hose string axis at times t_1, t_2, t_3 and t_4, and the comparison between numerical calculation and simulation results is shown in Figure 10 and Table 7.

Data of the maximum bending moment and the maximum axial force of the section in the calculation period are extracted respectively to draw a histogram of the maximum bending moment (Figure 11) and the maximum axial force of the section (Figure 12).

As can be seen from Figure 11, within 0~10 m, i.e. the maximum bending moment of the head hose is relatively concentrated, so the head hose is very easy to be bent and broken in the whole hose string. At the same time, when $x = 100\,\mathrm{m}$, the bending moment of the section of the hose string also appears abrupt change, so the rigidity design should be strengthened at the flange end of the interface between the tail hose and the FSO.

As shown in Figure 12, within 0~10 m, i.e. within the scope of the head hose, the head hose is subject to relatively concentrated maximum axial force, so the head hose is very vulnerable to bending fracture and tensile fracture in the whole hose string.

As for the displacement caused by wave load on the hose string, due to the influence of the dynamic

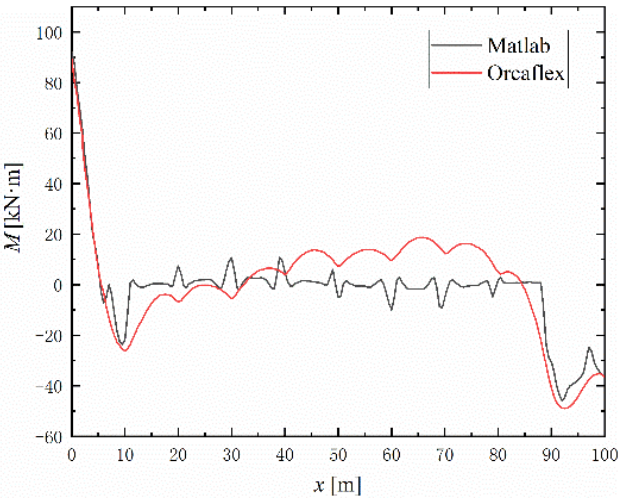

a) at time t = 0 s

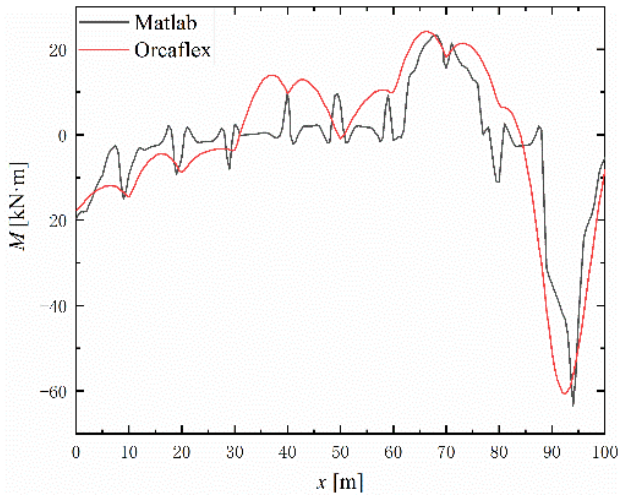

b) at time t = 1.4 s

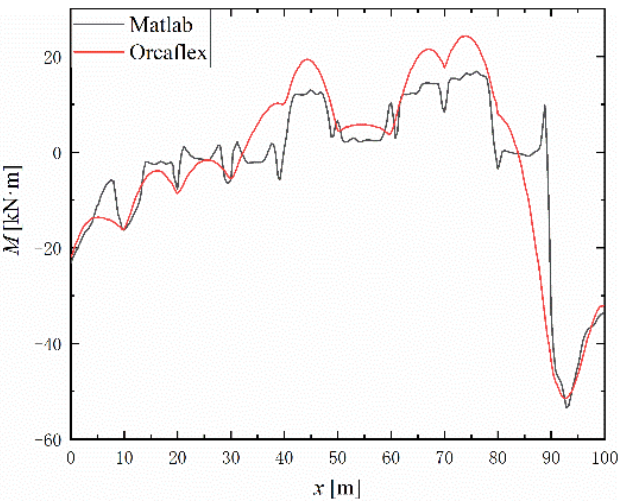

c) at time t = 2.8 s

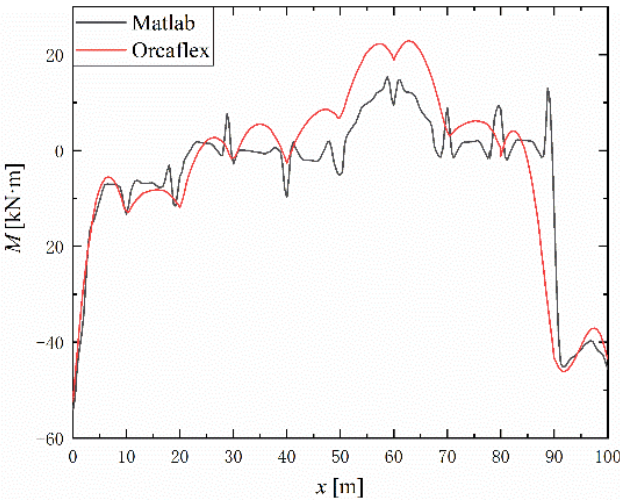

d) at time $t = 4.2$ s

Figure 10. The vertical bending moment comparison diagram of the floating hose string

boundary of the buoy, the floating hose string usually has a large displacement near the buoy, and the vertical displacement curve of the hose string shows a triangular function trend with the change of the direction displacement of the hose string gradually becoming flat. At the same time, due to the influence of the dynamic boundary of the FSO on the tail hose of the hose string, the last hose in the hose string is usually not subjected to wave load.

Due to the influence of the boundary between the buoy and the FSO, the maximum bending moment of the floating hose string mostly occurs at the joint of the buoy and the FSO. The bending moment in the middle part of the hose string shows a smooth transition trend. And the head hose of the floating hose string is subjected to a large bending moment, and the shear force at the interface between the head hose and the buoy flange is the largest. Therefore, a certain section stiffness transition structure should be designed at the joint of the head hose and the buoy, and the reinforcement end is designed to act as a shock absorber to absorb the horizontal motion of the buoy.

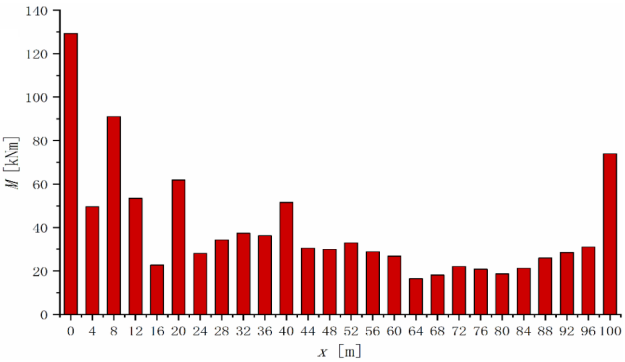

Figure 11. Maximum bending moment distribution of the cross section in one period

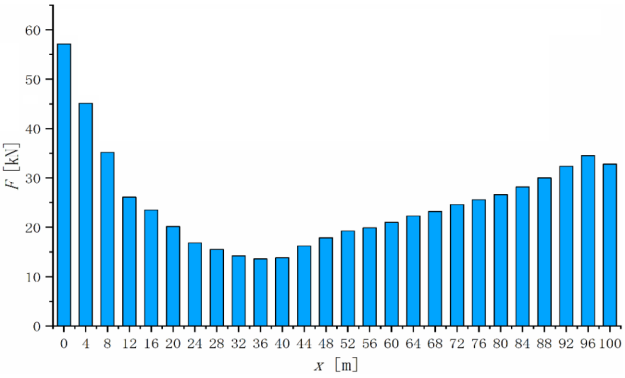

Figure 12. Maximum axial force distribution of the cross section in one period

5. CONCLUSION

In this paper, theoretical analysis and simulation calculation are carried out for the dynamic performance of floating oil delivery hose string in the overall offshore oil delivery system. The correctness of mechanical performance analysis is verified by Orcaflex software.

According to relevant assumptions, the bending differential calculation formula of floating hose string vibration is established. According to DNV report (2007) and based on the impact of actual working conditions and specific environmental parameters, the expression of vertical displacement of hose string under wave load is deduced.

Table 7: Vertical bending moment comparison of the hose string.

	Bending moment (kNm)							
	$t_1 = 0$ (s)		**$t_2 = 1.4$ (s)**		**$t_3 = 2.8$ (s)**		**$t_4 = 4.2$ (s)**	
	M^a	S^b	M^a	M^a	M^a	S^b	M^a	S^b
$x = 0$ (m)	94.3	90.093	−20.15	−17.675	−23.65	−21.984	−55.68	−53.418
$x = 100$ (m)	−35.8	−37.975	−5.23	−7.33	−33.2	−31.699	−46.38	−44.726
Maximum bending moment	94.3	90.093	−63.89	−60.8783	−53.8	−51.78	−55.68	−53.418

[a] Results obtained by mathematical models. [b] Results obtained by simulation software.

In this paper, the expression considering the influence of flange on the bending moment of the hose string is derived, and the vertical bending moment distribution of the hose string at different moments in a wave period is obtained by fitting with MATLAB. It was found that bending moment mutation occurred at each flange joint.

The displacement and bending moment of each section of the floating hose string are extracted by Orcaflex software. Through the comparison and analysis of theoretical numerical calculation results and simulation results, the feasibility of the theoretical numerical calculation method of bending moment vibration based on elastic foundation beam theory proposed in this paper to analyze the dynamic performance of the floating hose string is verified.

6. ACKNOWLEDGMENTS

The work was supported by the National Key Research and Development Plan (Grant no. 2016YFC0303704), National Natural Science Foundation of China (Grant no. 51879271), the 111 Project (B18054).

7. REFERENCES

1. AMAECHI, C.V., WANG, F.C., HOU, X.N., Ye, J.Q. *Strength of submarine hoses in Chinese-lantern configuration from hydrodynamic loads on CALM buoy*. Ocean Engineering, 2019, 171: 429-442.
2. BROWN, M.J., Elliott, L. *Two-dimensional dynamic analysis of a floating hose string*. Applied Ocean Research, 1988, 10(1): 20-34.
3. DET NORSKE VERTITAS. *Environmental Conditions and Environmental Loads*. Technical Report, 2007. Høvik, Norway
4. DYKE, P.P.G., MOSCARDINI, A.O., ROBSON E.H. *Offshore and Coastal Modelling*, Volume 12. Springer-Verlag, Berlin, Germany, 1985
5. Gao, Q., ZHANG, P., DUAN, M.L., YANG, X.Q., SHI, W.B., AN, C., Li, Z.L. *Investigation on structural behavior of ring-stiffened composite offshore rubber hose under internal pressure*. Applied Ocean Research, 2018, 79: 7-19.
6. O'DONOGHUE, T., HALLIWELL A.R. *Vertical bending moments and axial forces in a floating marine hose-string*. Engineering Structures, 1990, 12(2): 124-133.
7. ROVERI, F.E., SAGRILO, L.V.S., CICILIA F.B. *Case study on the evaluation of floating hose forces in a C.A.L.M. system*. Proceedings of the Twelfth International Offshore and Polar Engineering Conference, Kitakyushu, Japan, 2002, 26-31 May.
8. SAYED, F.B. and PATEL, M. H. *Mathematics of Flexible Risers Including Pressure and Internal Flow Effects*. Marine Structure-Special Flexible Risers Issue, 1992, 5: 121-150.
9. TONATTO, M.L.P., FORTE, M.M.C., TITA, V., AMICO, S.C. *Progressive damage modeling of spiral and ring composite structures for offloading hoses*. Materials & Design, 2016, 108: 374-382.
10. TONATTO, M.L.P., TITA, V., RICARDO, T.A., FORTE, M.M.C., AMICO, S.C. *Parametric analysis of an offloading hose under internal pressure via computational modeling*. Marine Structures, 2017, 51: 174-187.
11. TONATTO, M.L.P., TITA, V., FORTE, M.M.C., A.MICO S.C. *Multi-scale analyses of a floating marine hose with hybrid polyaramid/polyamide reinforcement cords*. Marine Structures, 2018, 60: 279-292.
12. ZHANG, S.F., CHEN, C., ZHANG, Q.X., ZHANG, D.M., ZHANG, F. *Wave loads computation for offshore floating hose based on partially immersed cylinder model of improved Morison formula*. The Open Petroleum Engineering Journal, 2015, 8: 130-137.
13. ZHOU, Y., DUAN, M.L., MA, J.M., SUN, G.M. *Theoretical analysis of reinforcement layers in bonded flexible marine hose under internal pressure*. Engineering Structures, 2018, 168: 384-398.

